Modulated crystal structure of chimney-ladder higher manganese silicides MnSi$_\gamma$ ($\gamma \sim 1.74$)

Yuzuru Miyazaki,[*] Dai Igarashi, Kei Hayashi, and Tsuyoshi Kajitani

Department of Applied Physics, Graduate School of Engineering, Tohoku University, 6-6-05 Aramaki Aoba, Aoba-ku, Sendai 980-8579, Japan

Kunio Yubuta

Advanced Research Center of Metallic Glasses, Institute for Materials Research, Tohoku University, 2-1-1 Katahira, Aoba-ku, Sendai 980-8577, Japan

The crystal structure of a polycrystalline sample of higher manganese silicide (HMS) has been determined by means of the (3+1)-dimensional superspace group approach. The structural parameters were refined with a superspace group of $I4_1/amd(00\gamma)00ss$ using powder neutron-diffraction data collected at 295 K. The compound belongs to a composite crystal family consisting of [Mn] and [Si] subsystems, with an irrational c-axis ratio (misfit parameter) of $\gamma = c_{Mn}/c_{Si} \sim 1.74$. Significant in-plane rotational modulation was revealed in the "chimney"-[Si] subsystem, while positional modulation in the "ladder"-[Mn] subsystem was only realized along c_{Mn}. The electronic structure of the sample was calculated on the basis of a commensurate approximation of the modulated structure using the full potential linearized augmented plane-wave method. The obtained band gap of $E_g \sim 0.6$ eV agreed well with the experimentally observed one. It appears that the band gap and density of states of the HMS samples depend on the positional modulation of the Si atoms. The various controversial formulas (for example, Mn_4Si_7, $Mn_{11}Si_{19}$, and so on) of the HMS phases reported thus far can be regarded as commensurate cases of a series of incommensurate MnSi$_\gamma$ phases in which the γ value ranges from ~ 1.70 to 1.75.

I. INTRODUCTION

Higher manganese silicides (HMSs) (MnSi$_{2-x}$) exhibit relatively high thermoelectric (TE) performance with the dimensionless figure-of-merit $ZT = S^2 T/\rho\kappa \sim 0.7$ at around 800 K, where S, ρ, κ, and T are the Seebeck coefficient, electrical resistivity, thermal conductivity, and absolute temperature, respectively.[1] Due to the natural abundance of the constituent elements and high-temperature oxidation resistance, these compounds are regarded as excellent potential p-type TE materials. Aoyama *et al.*[2] designed a TE module to generate electric power using HMSs as p legs and $Mg_2Si_{0.4}Sn_{0.6}$ as n legs. They reported that a conversion efficiency of 7.3% was achieved when the hot-side temperature was $T_h = 823$ K with an applied temperature difference of $\Delta T = 520$ K. To further optimize the TE properties of HMSs by the appropriate substitution of other elements, information on the crystal structure is critical. However, several structural formulas, e.g., Mn_4Si_7,[3] $Mn_{11}Si_{19}$,[4] $Mn_{15}Si_{26}$,[5] $Mn_{27}Si_{47}$,[6] were proposed as HMS phases and there has been a controversy as to whether the compounds are an identical phase or are a series of phases with different stacking periods. It is commonly recognized that all of these compounds are Nowotny chimney-ladder phases[7] which consist of a "chimney"-[Si] subsystem and a "ladder"-[Mn] subsystem. Electron diffraction studies have revealed that both of these subsystems have a common tetragonal a axis, but the c-axis lengths of the subsystems are usually different.[8] To account for the c-axis difference, a relatively large *commensurate* unit cell has been assumed. For this approach, a large number of independent positional parameters, usually containing more than nine atom sites,[3] is necessary to approximate the structure.

A superspace group approach is a beneficial way to describe an incommensurate compound by using a much reduced number of parameters. The positional modulation of the atoms can be expressed by means of Fourier terms of sine and cosine waves of the modulation functions. Yamamoto[9] first demonstrated that the most likely superspace group for the HMSs is $P:I4_1/amd:1\bar{1}ss$ (Mn) $W:P4/nnc:q\bar{1}q1$ (Si); in which the [Mn] subsystem has the three-dimensional (3D) space group of $I4_1/amd$, while the [Si] subsystem has that of $P4/nnc$. Using the incommensurate c-axis ratio $\gamma = c_{Mn}/c_{Si}$, the compounds can be expressed as MnSi$_\gamma$. However, to our best knowledge, no detailed structure analysis based on the superspace group approach has been reported thus far. We have employed a high-resolution neutron powder-diffraction technique to investigate the incommensurate crystal structure of the compound. Rietveld refinement, by considering up to the eighth order of the modulation waves, has precisely revealed the remarkable modulated helical arrangement of the chimney-[Si] subsystem along the c axis. The electronic structure of the sample has also been calculated on the basis of a commensurate approximation of the modulated structure using the full potential linearized augmented plane wave (FP-LAPW) method.

II. EXPERIMENTAL

Polycrystalline samples were prepared in a tetra-arc-type furnace under an Ar atmosphere using tungsten electrodes and a water-cooled copper hearth. Appropriate amounts of Mn (99.9%) and Si (99.99%) powders were mixed in an alumina mortar and pressed into pellets (30 mm diameter and 10 mm thick). The pellets were melted four times and turned

over each time in order to obtain full homogeneity. The buttons thus obtained were sealed in evacuated quartz tubes and annealed at 1273 K for 168 h.

Neutron powder-diffraction (ND) data were collected at 295 K using a Kinken powder diffractometer for high efficiency and high-resolution measurements (HERMES) (Ref. [10]) at the Institute for Materials Research (IMR), Tohoku University, installed at the JRR-3 reactor of the Japan Atomic Energy Agency (JAEA) at Tokai. A monochromatized incident neutron beam at $\lambda = 1.8265$ Å was employed. The ND data were analyzed with the JANA2000 software package.[11] The bound coherent scattering lengths used for the refinement were -3.730 fm (Mn) and 4.149 fm (Si), respectively. Crystal structures were drawn using the VESTA software[12] with the 3D coordinates derived from the PRJMS routine, bundled in the PREMOS 91 package.[9]

The band structure and the density of states (DOS) of the annealed samples were calculated on the basis of a commensurate approximation of the modulated structure using the WIEN2K software package based on the FP-LAPW method.[13] We applied exchange and correlation potentials using the generalized gradient approximation (GGA) of Perdew-Burke-Ernzerhof.[14] For the atomic spheres, the muffin-tin radii (R_{MT}) were chosen as 2.25 and 1.99 a.u. for Mn and Si, respectively. The number of plane waves was limited by a cutoff constant of $R_{MT}K_{max} = 7.0$, and the self-consistent calculation was carried out on a k mesh of 202 k points in the irreducible Brillouin zone (IBZ).

III. RESULTS AND DISCUSSION

A. Structure analysis

We assigned the [Mn] subsystem as subsystem 1 and adopted the most possible superspace group of $I4_1/amd(00\gamma)00ss$, equivalent to the full expression, $P:I4_1/amd:1\bar{1}ss$ (Mn) $W:P4/nnc:q\bar{1}q1$ (Si), originally described by Yamamoto.[9] Figure 1 illustrates the structural model of each subsystem. The [Mn] subsystem has 3D unit-cell dimensions of $a \sim 5.53$ Å and $c_{Mn} \sim 4.37$ Å, with the Mn atoms located at the origin ($4a$ sites) of the $I4_1/amd$ symmetry. The [Si] subsystem originally had 3D unit-cell dimensions of $a_{Si} \sim 3.91$ Å and $c_{Si} \sim 2.51$ Å with Si atoms at the origin ($2a$ sites) of the $P4/nnc$ space group. The unit vectors $\boldsymbol{a}_{Si}$ and $\boldsymbol{b}_{Si}$ in the [Si] subsystem were suitably transformed to $\boldsymbol{a} = \boldsymbol{a}_{Si} + \boldsymbol{b}_{Si}$ and $\boldsymbol{b} = -\boldsymbol{a}_{Si} + \boldsymbol{b}_{Si}$ to analyze the composite crystal structure. Simultaneously, the origin in the [Si] subsystem was shifted to $(-1/4, -1/4, -1/4)$, as shown in Fig. 1.

On the basis of the adopted superspace group, the translation parts are expressed as (0, 0, 0, 0; 1/2, 1/2, 1/2, 0) and the symmetry operations are represented as x_1, x_2, x_3, x_4; $-x_2, x_1+1/2, x_3+1/4, x_4$; $-x_1, x_2, x_3, x_4+1/2$; $-x_1, -x_2, x_3, x_4$; $-x_2, -x_1+1/2, x_3+1/4, x_4+1/2$; $x_2, -x_1+1/2, x_3+1/4, x_4$; $x_1, -x_2, x_3, x_4+1/2$; $x_2, x_1+1/2, x_3+1/4, x_4+1/2$; $-x_1, -x_2 +1/2, -x_3+1/4, -x_4$; $x_2, -x_1, -x_3, -x_4$; $x_1, -x_2+1/2, -x_3 +1/4, -x_4+1/2$; $x_1, x_2+1/2, -x_3+1/4, -x_4$; $x_2, x_1, -x_3, -x_4+1/2$; $-x_2, x_1, -x_3, -x_4$; $-x_1, x_2+1/2, -x_3+1/4, -x_4 +1/2$; $-x_2, -x_1, -x_3, -x_4+1/2$. The $(3+1)$-dimensional x_1,

[Mn] subsystem
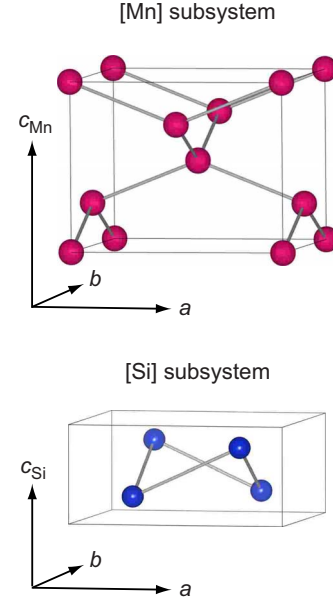
[Si] subsystem

FIG. 1. (Color online) Initial structural model for MnSi$_\gamma$. Both the [Mn] subsystem (upper) and the [Si] subsystem (lower) possess a tetragonal unit cell with the three-dimensional space-group symmetry of $I4_1/amd$ and $P4/nnc$, respectively. The origin in the [Si] subsystem was suitably shifted to $(-1/4, -1/4, -1/4)$ for composite structure analysis.

x_2, and x_3 coordinates correspond to the 3D coordinates x, y, and z in subsystem 1, and x_4 is the 3D fractional coordinate z in subsystem 2.

After several refinement cycles, positional modulation of the atomic sites was introduced, considering up to the eighth order of cosine and sine components of the Fourier terms A_n and B_n ($n = 1-8$). The positional modulation function $\bar{u}(\nu)$ of an atom is then expressed as

$$\bar{u}(\nu) = \sum_{n=1}^{8} \{A_n \cos 2\pi n\nu + B_n \sin 2\pi n\nu\},$$

where ν represents the fourth superspace coordinate without modulation in subsystem 1 or 2. For subsystem 1, ν is defined as $\gamma x_3 + t$, while ν equals $(1/\gamma)x_4 + t$ for subsystem 2. The parameter t is defined as the distance from 3D space and therefore corresponds to another expression of a $(3+1)$-dimensional superspace coordinate.

Figure 2 shows the observed, calculated, and difference profiles of the HERMES data for MnSi$_\gamma$ measured at 295 K. The short vertical lines below the patterns indicate the peak positions of possible Bragg reflections. Small peaks at $2\theta \sim 32.5°$, $40.5°$, and $53.0°$, derived from the second phase MnSi, were excluded in the refinement cycles. The final R factors were $R_{wp} = 9.5\%$ and $R_p = 6.8\%$, and the lattice parameters were refined to be $a = 5.5271(2)$ Å, $c_{Mn} = 4.3668(2)$ Å, and $c_{Si} = 2.5153(3)$ Å. The numbers in parentheses represent the estimated standard deviations of the last significant digit. The resulting c-axis ratio was $\gamma = 1.7361(1)$, different from that of any commensurate HMSs.[3–6] Table I summarizes the atomic coordinates and equivalent isotropic displacement
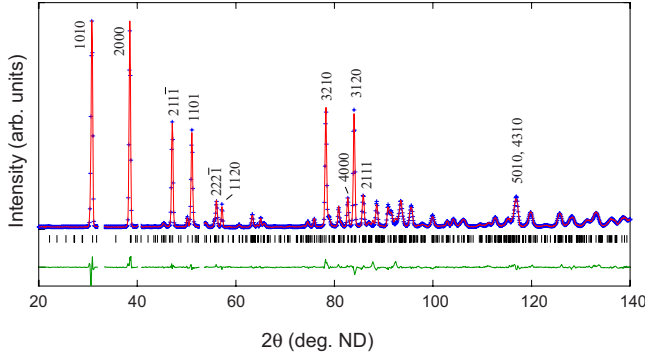
FIG. 2. (Color online) Observed, calculated, and difference patterns of powder neutron-diffraction data for MnSi$_\gamma$ measured at 295 K. Short vertical lines below the patterns indicate positions of Bragg reflections. The difference between the observed and calculated intensities is shown below the vertical lines. The peaks denoted as $hkl0$ and $hk0m$ are the fundamental reflections derived from the [Mn] and [Si] subsystems, respectively, while the $hklm$ peaks are satellite reflections.

parameters, U_{eq}, for the fundamental structure of MnSi$_\gamma$ at 295 K.

B. Details of modulated structure

Table II summarizes the refined Fourier amplitudes for the positional parameters together with the anisotropic displacement parameters of each atom. Due to the superspace group symmetry, the number of refinable parameters of the Fourier terms is limited. Only even terms of the sine wave along the z direction, i.e., B_{2z}, B_{4z}, B_{6z}, and B_{8z}, are allowed for the Mn atoms. In contrast, odd terms of the sine and cosine waves are allowed for both the x and y components for the Si atoms along with B_{4z} and B_{8z} terms. The amplitudes of each cosine wave component in the $x-y$ plane, such as A_{1x} and A_{1y}, are equal, while those of each sine wave are equal but their signs are opposite.

Figure 3 shows the revealed positional modulations for the x, y, and z coordinates of each atom plotted against the fourth superspace coordinate ν. The right vertical axes are rescaled to represent the displacement (in angstroms) for each atom. All the displacements are periodic in the interval $0 \leq \nu \leq 1.0$. For the Mn atoms, positional modulation is only allowed in the z direction and the maximum displacement

TABLE I. Atomic coordinates and equivalent isotropic atomic displacement parameters, U_{eq}, for the fundamental structure of MnSi$_\gamma$ at 295 K.

	x (=x_1)	y (=x_2)	z (=x_3)	U_{eq} (Å^2)
Subsystem 1: [Mn]	0	0	0	0.0153(8)
	x (=x_1)	y (=x_2)	z (=x_4)	U_{eq} (Å^2)
Subsystem 2: [Si]	1/4	1/4	1/4	0.0185(7)

TABLE II. Refined positional modulation wave components and anisotropic displacement parameters, U_{ij}, for MnSi$_\gamma$.

Subsystem 1: [Mn]	x (=x_1)	y (=x_2)	z (=x_3)
B_2	0	0	−0.0172(10)
B_4	0	0	0.020(3)
B_6	0	0	0[a]
B_8	0	0	0[a]

$U_{11} = U_{22} = 0.0136(14)$ (Å^2)
$U_{33} = 0.019(2)$ (Å^2)

Subsystem 2: [Si]	x (=x_1)	y (=x_2)	z (=x_4)
A_1	0.0771(2)	=A_{1x}	0
B_1	=A_{1x}	=−A_{1x}	0
A_3	0.0101(2)	=A_{3x}	0
B_3	=−A_{3x}	=A_{3x}	0
B_4	0	0	−0.0395(16)
A_5	−0.0028(4)	=A_{5x}	0
B_5	=A_{5x}	=−A_{5x}	0
A_7	0[a]	=A_{7x}	0
B_7	=−A_{7x}	=A_{7x}	0
B_8	0	0	0.010(4)

$U_{11} = U_{22} = 0.0174(14)$ (Å^2)
$U_{33} = 0.021(2)$ (Å^2)

[a]Fixed at 0 because their deviations from the present values were not significant.

($\sim$0.12 Å) from $z=0$ is recognized at $\nu \sim 0.18$, 0.32, 0.68, and 0.82. The displacement of Si atoms along z is comparable to that of the Mn atoms and the maximum displacement of ($\sim$0.13 Å) from $z=1/4$ can be seen at $\nu \sim 0.03$, 0.19, 0.28, etc. Based on the large sine and cosine components, the rotational modulation in the x and y directions is significant for the Si atoms. Both the modulation waves in x and y are identical with the phase shift of $\Delta \nu = 1/4$. The maximum displacement of $\sim$0.54 Å from $x=1/4$, equivalent to $\Delta x \sim 0.1$, is realized at $\nu \sim 0.48$ and 0.98, and at $\nu \sim 0.23$ and 0.73 from the $y=1/4$ position. Similar rotational modulation is reported for relating chimney-ladder compounds, such as $(Mo_{1-x}Rh_x)Ge_\gamma$ (Ref. 18) and $(Cr_{1-x}Mo_x)Ge_\gamma$.[19] Interestingly, the deviation from the fundamental position, Δx and Δy, is also $\sim$0.1 in these compounds, although the a-axis lengths of these phases are much larger ($a \sim 5.9$ Å) than that in the present compound.

In Fig. 4 we show the revealed modulated composite structure of MnSi$_\gamma$ at 295 K. The upper figure illustrates the c-axis projection to represent the helical arrangement of the chimney-Si atoms. The lower figure depicts the atoms within $5 \times c_{Mn}$ length. The seven squares on the right represent slices of the first to seventh layers of Si atoms from the origin. The first layer of Si atoms corresponds to $\nu = (1/\gamma)x_4 + t = (1/\gamma) \times (1/4) - 0.1440 = 0$. As deduced from Fig. 3, the coordinates at $\nu = 0$ are around $(x, y) = (0.35, 0.23)$. Since there is a twofold axis at $(1/2, 1/2)$ parallel to the c axis, the other Si atom in the first layer is
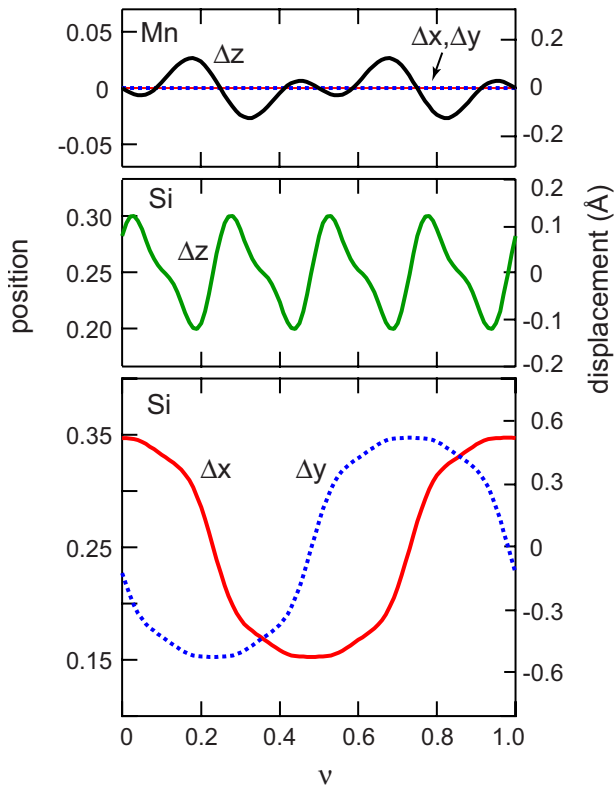
FIG. 3. (Color online) Revealed positional modulations of the Mn and Si atoms plotted as a function of the fourth superspace coordinate ν. The right vertical axes are rescaled to represent the displacement for each atom.

located at around (0.65, 0.77). Similarly, the third ($x_4=5/4$) and fifth ($x_4=9/4$) layers of Si atoms, corresponding to ν $=0.576$ and 0.152 ($\equiv 1.152$), are located at around (0.16, 0.32), (0.84, 0.68) and (0.32, 0.16), (0.68, 0.84), respectively. By symmetry, the coordinates of even numbered layers can be obtained as ($-x$, y) and (x,$-y$). The second ($x_4=3/4$) and fourth ($x_4=7/4$) layers of Si atoms, corresponding to ν $=0.288$ and 0.864, are located at around (0.19, 0.85), (0.81, 0.15) and (0.33, 0.67), (0.67, 0.33), respectively. The z coordinates of Si and Mn atoms in the modulated structure can also be calculated in a similar way.

Figure 5 shows interatomic distances plotted as a function of the internal coordinate t. The two periodic curves around the distance of 3.0 Å in Fig. 5(a) represent the nearest four Mn-Mn distances, wherein each curve is duplicated because of the two equidistant bonds. The nearest Mn-Mn distances, ranging from 2.92 to 3.01 Å, are relatively longer than that expected from the atomic radius of Mn, $r_{Mn}=1.24$ Å.[15] However, such long distances have been reported in the complicated structure of α-Mn,[16] wherein the Mn-Mn distances vary from 2.24 to 2.96 Å and in the intermetallic compound Mn$_5$Si$_3$ with a distance of 2.96 Å.[17] In the case of the Mn-Si bonds, each Mn atom is coordinated to eight Si atoms, as seen in Fig. 4. The four curves around 2.4 Å in Fig. 5(a) represent the nearest eight Mn-Si distances, with each curve duplicated because of equidistant Mn-Si bond pairs. At $t=0$, the Mn atom has eight Si neighbors with $d_{Mn-Si} \sim 2.4$ Å, which is the typical Mn-Si bond distance on the basis of the
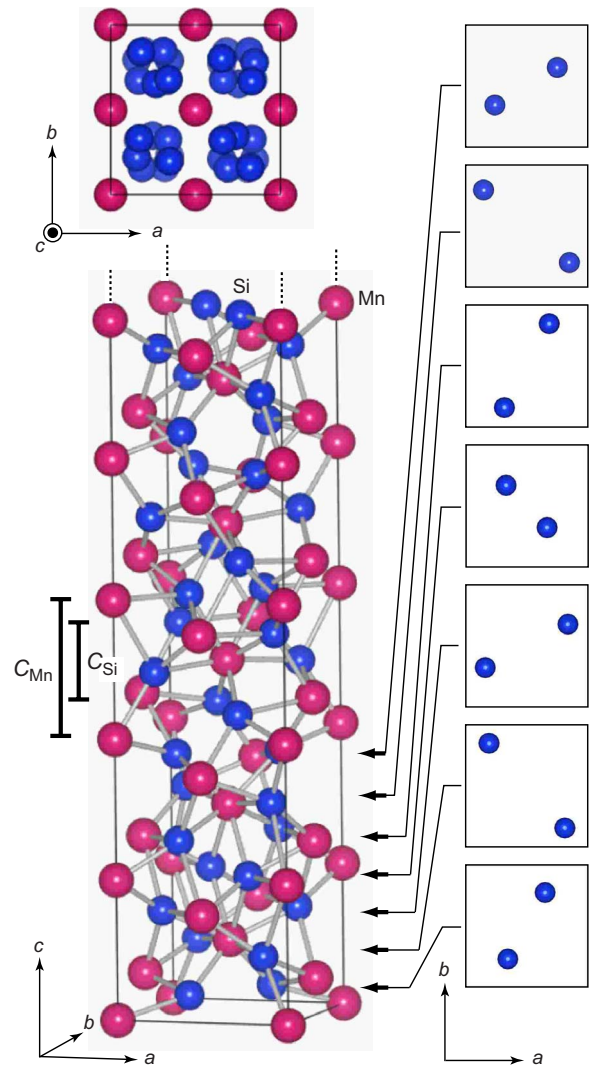
FIG. 4. (Color online) Revealed modulated composite structure of MnSi$_\gamma$ at 295 K. The upper figure is a c-axis projection to illustrate the rotational arrangement of chimney-Si atoms. The lower figure depicts the atoms within $5 \times c_{Mn}$ lengths. The seven squares on the right are slices of the first to seventh layers of Si atoms from the origin.

metallic radii of Mn and Si ($r_{Si}=1.17$ Å).[15] With increasing t, the four bonds (two curves) become shorter toward ~ 2.2 Å and the remaining four bonds become longer. Accordingly, two Si atoms detach at $t \sim 0.25$ but the other two Si atoms attach to the Mn atom. In this way, the Mn atom is always bounded to eight Si atoms within the distance of <2.8 Å. The nearest Si-Si distances show a periodic alteration as a function of t, as shown in Fig. 5(b), because they belong to the same subsystem. The minimum distance of 2.46 Å is slightly longer than that expected from r_{Si} of 2.34 Å. The observed longer homoatomic Mn-Mn and Si-Si distances as well as the compatible heteroatomic Mn-Si distances on the basis of r_{Mn} and r_{Si} can be a characteristic of the chimney-ladder phases. A similar observation has also been reported for other chimney-ladder compounds including (Mo$_{1-x}$Rh$_x$)Ge$_\gamma$,[18] (Cr$_{1-x}$Mo$_x$)Ge$_\gamma$,[19] and ZrBi$_\gamma$.[20]
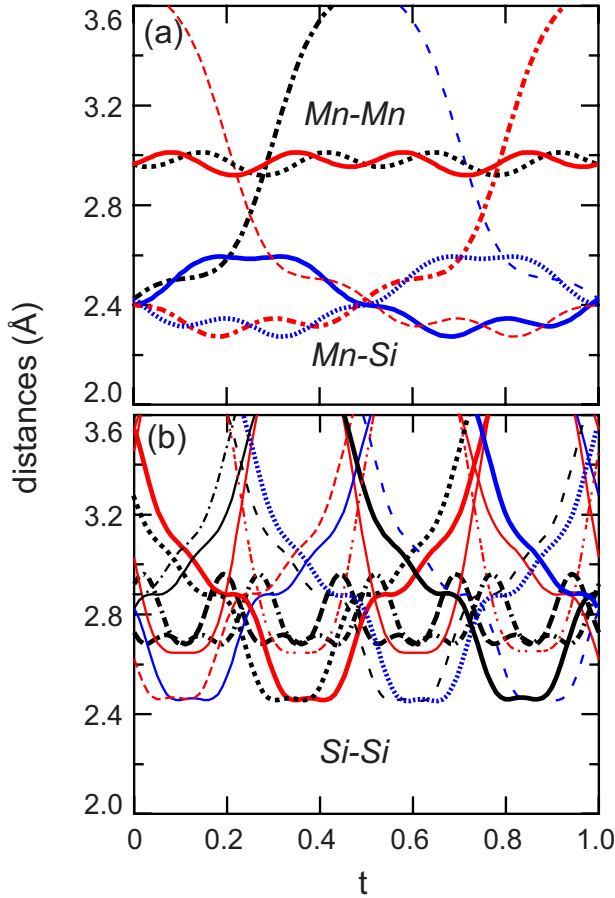
FIG. 5. (Color online) Interatomic distances, (a) Mn-Mn and Mn-Si, (b) Si-Si, as a function of the fourth superspace coordinate t for MnSi$_\gamma$ at 295 K.

C. Structure comparison between MnSi$_\gamma$ and other HMSs

In principle, the superspace group approach described above can also be applicable to the reported commensurate structure of HMSs. Toward the uniform treatment of the crystal structure of the present MnSi$_\gamma$ and other HMSs, we will first convert the 3D coordinates of Mn$_4$Si$_7$ (Ref. 3) to ν, which depends either on x_3 or x_4 by definition. The Mn$_4$Si$_7$ phase can be regarded as a case of $\gamma = 7/4 = 1.75$, wherein $4c_{Mn}$ exactly equals $7c_{Si}$; the 3D unit cell consists of the stacking of four [Mn] subsystems and intervening seven [Si] subsystems. Let us consider the [Si] subsystem closest to the origin. The Si atom at Si1 $(8j)$ sites with $(0.15715, 0.2015, 0.11253)$ is converted to $(0.15715, 0.2015, x_4 + \delta)$ in the [Si] subsystem. Since the Si atom is located at the second $(x_4 = 3/4)$ layer, we obtain $\nu = (1/\gamma) \times x_4 - (4/7) \times 1/4 = 0.286$ and $3/4 + \delta = 7 \times 0.11253 = 0.788$. Similarly, the Si atom at Si4 $(8j)$ sites with $(0.34518, 0.2274, 0.9620)$ is converted to $(0.34518, 0.2274, 27/4 + \delta')$ with $\nu = 0.714 \ (\equiv 3.714)$. In this case, $27/4 + \delta'$ equals $7 \times 0.9620 = 6.734$ in the [Si] subsystem, corresponding to $z = 0.734$ in the seventh [Si] subsystem from the origin. By applying all the symmetry operations to the Mn1-Mn5 and Si1-Si4 sites, the equivalent positions close to Mn $(0, 0, 0)$ and Si $(1/4, 1/4, 1/4)$ in each subsystem can be obtained as filled circles shown in Fig. 6.

On the basis of this manner, those equivalent positions of Mn$_{11}$Si$_{19}(\gamma = 1.7\dot{2}\dot{7})$,[4] Mn$_{15}Si_{26}(\gamma = 1.7\dot{3})$,[5] and Mn$_{27}Si_{47}(\gamma$
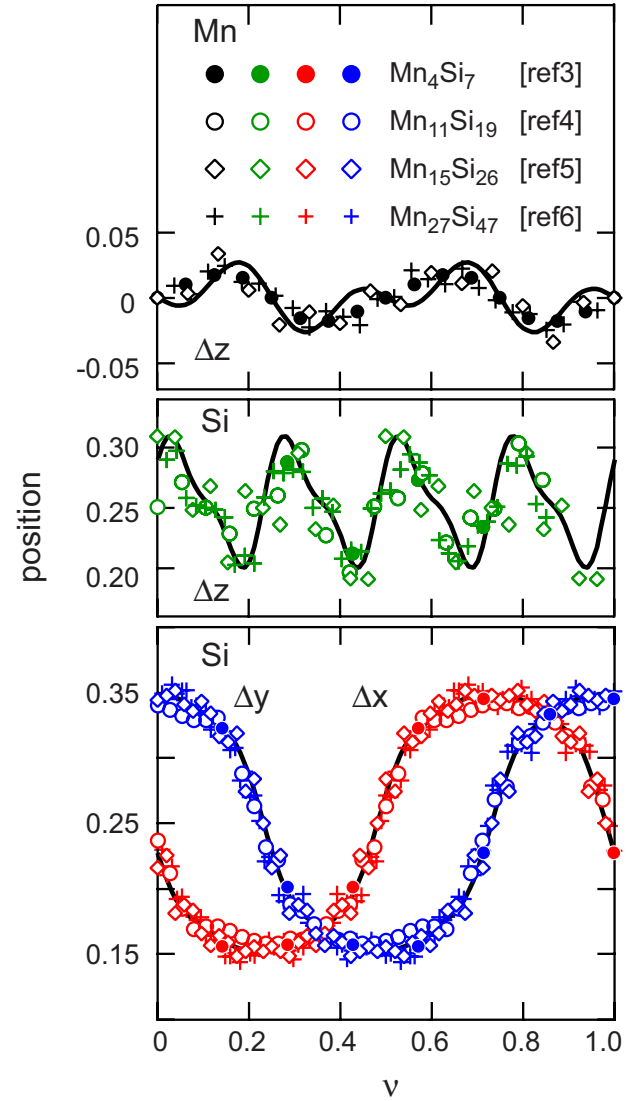
FIG. 6. (Color online) The converted coordinates of Mn at $\sim(0,0,0)$ and Si at $\sim(1/4,1/4,1/4)$ in each subsystem of HMSs plotted as a function of the superspace coordinate ν. Data are taken from Refs. 3–6. Solid lines are the data of the present incommensurate MnSi$_\gamma$ [$\gamma = 1.7361(1)$].

$= 1.7\dot{4}0\dot{7}$) (Ref. 6) are, respectively, converted to the marks as a function of ν as shown in Fig. 6. The solid line(s) in each panel correspond(s) to the one(s) shown in Fig. 3 but the x and y lines are interchanged to preserve the original (x, y) coordinates reported in Refs. 3–6. Among the points, all the x and y coordinates in the [Si] subsystem are excellently superposed on the two *universal* lines, suggesting that the manner of helical arrangement of Si atoms is almost identical and independent of the γ values in all HMSs. In contrast, the z coordinates of Mn and Si atoms deviate from the periodic solid lines of the present sample. It would be, however, reasonable to consider different shapes of curves, i.e., different B_z terms, to fit the z coordinates for each HMS because the stacking periodicity might be dependent on γ, even though the z coordinates of Si atoms appear to be difficult to fit periodic waves except for the Mn$_4$Si$_7$ phase. In other words, such a deviation from the periodic lines, ob-

TABLE III. Commensurate structure model used for calculation of the electronic structure for $MnSi_\gamma$. Space group: $P2$ (No. 2, unique axis c), $a=b=5.5271$ Å, $c=4c_{Mn}=17.4672$ Å, $\alpha=\beta=\gamma=90°$.

Atom	Site	x	y	z
Mn1	1a	0	0	0
Mn2	1a	0	0	0.2471
Mn3	1a	0	0	0.4979
Mn4	1a	0	0	0.7430
Mn5	1b	1/2	0	0.1943
Mn6	1b	1/2	0	0.4396
Mn7	1b	1/2	0	0.6900
Mn8	1b	1/2	0	0.9373
Mn9	1c	0	1/2	0.0605
Mn10	1c	0	1/2	0.3050
Mn11	1c	0	1/2	0.5634
Mn12	1c	0	1/2	0.8080
Mn13	1d	1/2	1/2	0.1298
Mn14	1d	1/2	1/2	0.3744
Mn15	1d	1/2	1/2	0.6326
Mn16	1d	1/2	1/2	0.8772
Si1	2e	0.3478	0.2286	0.0408
Si2	2e	0.1936	0.8450	0.1149
Si3	2e	0.1606	0.3261	0.1821
Si4	2e	0.3360	0.6685	0.2541
Si5	2e	0.3176	0.1574	0.3193
Si6	2e	0.1532	0.7900	0.3887
Si7	2e	0.2509	0.3482	0.4682
Si8	2e	0.3467	0.7914	0.5474
Si9	2e	0.1816	0.1576	0.6165
Si10	2e	0.1643	0.6681	0.6845
Si11	2e	0.3397	0.3255	0.7537
Si12	2e	0.3053	0.8452	0.8210
Si13	2e	0.1521	0.2302	0.8955
Si14	2e	0.2731	0.6522	0.9771

served in $Mn_{11}Si_{19}$, $Mn_{15}Si_{26}$, and $Mn_{27}Si_{47}$, can be treated as a stacking fault in a regular periodicity along the c axis.

D. Band structure and density of states of commensurately approximated $MnSi_\gamma$

In order to evaluate the electronic structure of the $MnSi_\gamma$ [$\gamma=1.7361(1)$] sample, the incommensurate structure was converted onto 3D space. We adopted the approximate unit cell of $a \times a \times 4c_{Mn}$, in which $4c_{Mn}=17.4672$ Å roughly equals $7c_{Si}=17.6071$ Å. The space group and fractional coordinates of the Mn and Si atoms, derived from the StructGen™ and Initialize calc processes in the calculation,[13] are summarized in Table III. The approximated structure contains 16 Mn sites ($1a$-$1d$) and 14 Si sites ($2e$), with the monoclinic $P2$ space group ($\alpha=\beta=\gamma=90°$) which has the unique axis through (1/2, 1/2, 0) parallel to the c axis.
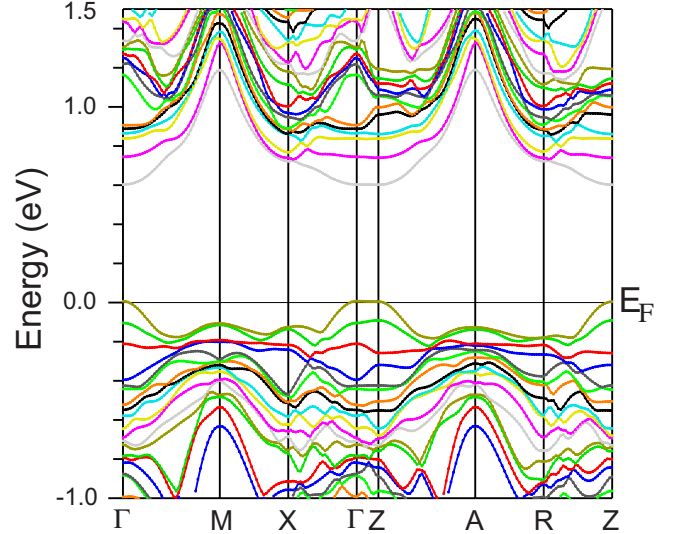
FIG. 7. (Color online) The band structure of $MnSi_\gamma$ [$\gamma=1.7361(1)$] based on the commensurate approximation of the incommensurate structure.

The calculated band structure along several high-symmetry directions of IBZ in the range of $-0.5 \leq E \leq 1.5$ eV is shown in Fig. 7. The $MnSi_\gamma$ [$\gamma=1.7361(1)$] sample is a semiconductor with a band gap of ~0.6 eV. However, it is difficult to determine whether the band gap is direct or indirect because of the flat bands along the Γ-Z direction. The indirect band gap between the valence-band maximum in the Γ point and the conduction-band minimum in the Z point is 0.595 eV, while the direct band-gap values in the Γ point and Z point are 0.596 and 0.597 eV, respectively. It should be noted here that the spin polarized calculation was also attempted, but we never obtained any recognizable magnetic moment in the present sample. The overall feature of the band structure is qualitatively in good agreement with the recently reported band structure of Mn_4Si_7 by Migas *et al.*[21] One difference is that their band gap of ~0.77 eV is even larger than that obtained in the present study. This difference is attributable to the different structure model adopted. The lattice parameters used for our calculation are slightly larger than those adopted by Migas *et al.* of $a=5.510$ Å and $c=17.418$ Å. According to our calculation based on the refined structure model of an "as-melted" sample, which is from the same batch as the present sample but *without* annealing, the dispersion of the lowest (161th) conduction band was lowered and we obtained an indirect band gap of 0.537 eV. Both the as-prepared and annealed samples had identical a and c_{Mn} lengths within the estimated standard deviations but a smaller misfit ratio of $\gamma=1.7326(1)$ for the as-melted sample, yielding a different stacking periodicity of Si atoms [i.e., $B_4=-0.0441(19)$ and $B_8=0.017(4)$] while maintaining that of the Mn atoms. Migas *et al.*[21] further investigated the effects of stacking faults by introducing additional Si atom and observed a significant change in the band dispersion in the vicinity of the band gap, as well as a reduced band-gap value of 0.40 eV. Such defect structures can be regarded as the cases with a large deviation from the periodic lines of the z coordinates of Si atoms
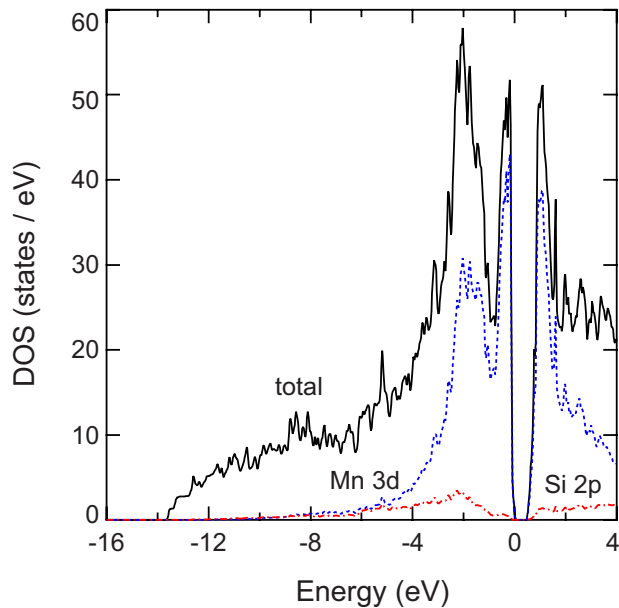
FIG. 8. (Color online) The total DOS and the contribution of Mn-3d and Si-2p bands of MnSi$_\gamma$ with $\gamma = 1.7361(1)$ based on the commensurate approximation of the incommensurate structure.

shown in Fig. 6. Judging from these observations, the dispersion of the lower-lying conduction bands and the valence-band maximum are relatively sensitive to the lattice parameters and/or the distribution of the atoms. Previously reported contradicting band-gap data, ranging from 0.32 to 0.70 eV,[22–25] could be attributable to small differences in the structural parameters and local arrangement of atoms, in particular Si, originating from a slight variation in γ.

In Fig. 8, we show the energy dependence of the total DOS and the contributions of the Mn-3d and Si-2p bands of MnSi$_\gamma$ with $\gamma = 1.7361(1)$ based on the commensurate approximation of the incommensurate structure. The sharp peak ranging from -0.7 to the Fermi level (E_F) is dominantly a Mn-3d character, consistent with the experimentally observed p-type semiconducting behavior. Such a steep DOS near E_F is prerequisite for realizing a good p-type thermoelectric material because S is proportional to the energy derivative of DOS at E_F. A broad peak at $E=-4$ to -1 eV can be assigned and characterized to the Mn-3d and Si-2p bonding states. Similar to the band structure, the obtained DOS curves also resemble those reported by Migas *et al.*[21] However, the DOS and the Mn-3d contribution in the conduction band at $E=0.6$ to 1.3 eV are almost equal to the peaks at $E \sim E_F$ in the present sample. Hence, a partial substitution of Mn with a heavier element is expected to raise E_F to the conduction-band bottom and would show comparable n-type thermoelectric performance to the p-type counterpart. Earlier reports have indicated that the Mn atoms can be substituted with Fe up to $\sim 30\%$ and n-type conduction was in fact observed.[26–28] Nevertheless, the absolute value of $S \sim -70$ μV at room temperature is around half of that of the p-type analog. Moreover, the ρ value for the n-type samples is approximately 1 order of magnitude higher than that of the p-type HMSs, leading to a ZT value far below 0.1 at 300 K. Such inferior performance of the n-type HMS has been ascribed to low carrier mobility due to the potential randomness of the substituted Fe atoms distributed in the Mn subsystem.[28] To improve the thermoelectric properties of n-type HMS, a materials design based on the modulated structure analyses combined with the electronic structure and DOS calculation for the Fe-substituted samples is currently underway.

IV. SUMMARY AND CONCLUSIONS

The present structure analysis has revealed that the c-axis ratio, γ, which also indicates the stoichiometry of the MnSi$_\gamma$ samples, is generally an irrational number around 1.74. The γ value can be varied slightly, in the range between ~ 1.70 and 1.75, by changing the starting composition of the Mn:Si mixtures and the thermal history of the samples. A small difference in γ causes a different periodicity of the Si atoms and therefore their modulation, while little modulation is recognized for Mn atoms. Such a difference in the atomic arrangement affects the magnitude of the band gap and the density of states near the Fermi level, causing a small change in the thermoelectric properties. If we can appropriately control the structural parameters by substitution of Mn and/or Si sites or by introducing stacking faults, etc., further improvement in the thermoelectric properties, together with the preparation of a potential n-type thermoelectric material, can be realized.

*miya@crystal.apph.tohoku.ac.jp

[1] M. I. Fedorov and V. K. Zaitsev, in *Thermoelectrics Handbook*, edited by D. M. Rowe (CRC Press, Boca Raton, 2006), Chap. 31, p. 3.

[2] I. Aoyama, H. Kaibe, L. Rauscher, T. Kanda, M. Mukoujima, S. Sano, and T. Tsuji, Jpn. J. Appl. Phys., Part 1 **44**, 4275 (2005).

[3] U. Gottlieb, A. Sulpice, B. Lambert-Andron, and O. Laborde, J. Alloys Compd. **361**, 13 (2003).

[4] O. Schwomma, H. Nowotny, and A. Wittman, Monatsh. Chem. **94**, 681 (1963).

[5] H. W. Knott, M. H. Mueller, and L. Heaton, Acta Crystallogr. **23**, 549 (1967).

[6] G. Zwilling and H. Nowotny, Monatsh. Chem. **104**, 668 (1973).

[7] H. Nowotny, in *The Chemistry of Extended Defects in Non-Metallic Solids*, edited by L. Eyring and M. O'Keeffe (North Holland, Amsterdam, 1970).

[8] H. Q. Ye and S. Amelincks, J. Solid State Chem. **61**, 8 (1986).

[9] A. Yamamoto, Acta Crystallogr. A **49**, 831 (1993).

[10] K. Ohoyama, T. Kanouchi, K. Nemoto, M. Ohashi, T. Kajitani, and Y. Yamaguchi, Jpn. J. Appl. Phys., Part 1 **37**, 3319 (1998).

[11] V. Petricek, M. Dusek, and L. Palatinus, *JANA2000 The Crystallographic Computing System* (Institute of Physics, Praha, Czech Republic, 2000).

[12] K. Momma and F. Izumi, J. Appl. Crystallogr. **41**, 653 (2008).

[13] P. Blaha, K. Schwarz, G. K. H. Madsen, D. Kvasnicka, and J. Luitz, *WIEN2k, An Augumented Plane Wave + Local Orbital Program for Calculating Crystal Properties* (K. Schwarz, Techn, Univ., Wien, Austria, 2001).

[14] J. P. Perdew, K. Burke, and M. Ernzerhof, Phys. Rev. Lett. **77**, 3865 (1996).

[15] *Agne Periodic Table*, edited by T. Inoue, S. Chikazumi, S. Nagasaki, and S. Tanuma (AGNE Technology Center, Tokyo, 2001).

[16] A. J. Bradley and J. Thewlis, Proc. R. Soc. London, Ser. A **115**, 456 (1927).

[17] P. J. Brown, J. B. Forsyth, V. Nunez, and F. Tasset, J. Phys.: Condens. Matter **4**, 10025 (1992).

[18] F. E. Rohrer, H. Lind, L. Eriksson, A.-K. Larsson, and S. Lidin, Z. Kristallogr. **215**, 650 (2000).

[19] F. E. Rohrer, H. Lind, L. Eriksson, A.-K. Larsson, and S. Lidin, Z. Kristallogr. **216**, 190 (2001).

[20] M. Boström, H. Lind, S. Lidin, R. Miewa, and Y. Grin, Solid State Sci. **8**, 1173 (2006).

[21] D. B. Migas, V. L. Shaposhnikov, A. B. Filonov, V. E. Borisenko, and N. N. Dorozhkin, Phys. Rev. B **77**, 075205 (2008).

[22] E. N. Nikitin, V. I. Tarasov, and P. V. Tamarin, Sov. Phys. Solid State **11**, 187 (1969).

[23] I. Nishida, J. Mater. Sci. **7**, 1119 (1972).

[24] I. Kawasumi, M. Sakata, I. Nishida, and K. Masumoto, J. Mater. Sci. **16**, 355 (1981).

[25] C. Krontiras, K. Pomoni, and M. Roilos, J. Phys. D **21**, 509 (1988).

[26] E. N. Nikitin and V. I. Tarasov, Sov. Phys. Solid State **13**, 2938 (1971).

[27] V. I. Tarasov, E. N. Nikitin, and L. N. Shumilova, Izv. Akad. Nauk SSSR, Neorg. Mater. **11**, 1038 (1975).

[28] V. K. Zaitsev, V. I. Tarasov, and A. A. Adilbekov, Sov. Phys. Solid State **17**, 370 (1975).